Harmonic Photoacoustic Imaging: a new approach using ultrasound detector harmonic resonances to improve image resolution in photoacoustics

Rogier R. Wildeboer
Supervisors: W. Xia, W. Steenbergen and S. Manohar
Biomedical Photonic Imaging Group,
MIRA Institute for Biomedical Technology and Technical Medicine, University of Twente
contact: r.r.wildeboer@student.utwente.nl

ABSTRACT

Photoacoustics is an emerging imaging technology in biomedicine, in which absorption of laser pulses by structures in tissue generate detectable acoustic signals. While conventionally only the fundamental frequency bandwidth (FBW) of the ultrasound detector has implicitly received attention in determining the imaging resolution, we show that it is also important to consider the contribution of detector harmonic resonances. Further, we introduce an approach where we combine image reconstructions from fundamental FBW signals with reconstructions from harmonic signals, to achieve improved image quality. We validate this approach using simulations and phantom measurements.

Keywords
photoacoustic imaging, tomography, ultrasound detector, harmonic resonances, multiple bandwidth, spatial resolution

INTRODUCTION

Photoacoustics (PA), also known as optoacoustics, is a non-invasive and non-ionizing imaging technique that is used increasingly in biomedicine. PA signals are produced when chromophores within tissue are irradiated by a light pulse [1,2]. In tissue, the energy of the laser pulse is absorbed to different extents and consequently converted into heat. As the material expands thermo-elastically, ultrasound (US) waves are generated. In PA tomography, pressure signals in the time domain are recorded by an array of US detectors around the surface of the sample and subsequently used to reconstruct its internal structure [3]. This method has been used to image large organs to organelles and promises applications in breast cancer imaging, melanoma visualization, small animal imaging and detection of rheumatoid arthritis [2,4].

The acoustic waves that arrive at the surface of the object are usually measured with piezoelectric US detectors. The detection mechanism is based on the piezoelectric effect, in which an electrical potential is created by mechanical displacement within a piezoelectric crystal as it starts resonating with the arriving acoustic wave. That is, mainly in the fundamental resonant frequency of the crystal, and to lower extents in its higher harmonic frequencies.

PA image resolution is dictated by this fundamental frequency bandwidth (FBW) as well as on image reconstruction algorithms used. As is demonstrated theoretically [5] and experimentally [6], the higher the fundamental frequency of the detector, the higher the spatial resolution. Generally, the achievable resolution is estimated as half of the fundamental frequency wavelength [7]. In PA tomography, spatial resolution can be subdivided in axial (depth) and lateral (tangential) resolution. Axial resolution is measured perpendicular to the surface of the detector, while lateral resolution is positioned parallel to the surface. Theoretically, resolution can be improved by broadening the FBW while moving the fundamental to higher frequencies, and reducing the size of the transducer. However, theseentail fabrication challenges and increase sensitivity to noise.

In contrast to ultrasound imaging where a single known narrow frequency band is (sent into tissue and) measured, in PA generated frequencies depend on the size of the structure being imaged, ranging from hundreds of kHz to tens of MHz. Smaller objects will produce US signals with higher frequencies [1,2]. Frequencies above the cut-off frequency of the detector's bandwidth are not considered specifically in PA [6]. We propose that higher harmonics in the frequency response of the detector contain this

SRC 2011, November 23–24, 2011, Eindhoven, The Netherlands.

additional, more accurate spatial information. By measuring and enhancing signals with the help of these harmonics in addition to the fundamental signal, it should be possible to extract better resolutions and image smaller structures accurately.

In this paper, we investigate the validity of the hypothesis using both simulations and experiments. Specifically we (1) performed HPI simulations using numerical phantoms and evaluated the precision of the simulation model, (2) designed and developed an elegant and easy-to-use 2D-phantom for spatial resolution determination and imaged the phantom applying the the principle of harmonic photoacoustic imaging (HPI) and (3) assessed resolution (and image quality) improvement.

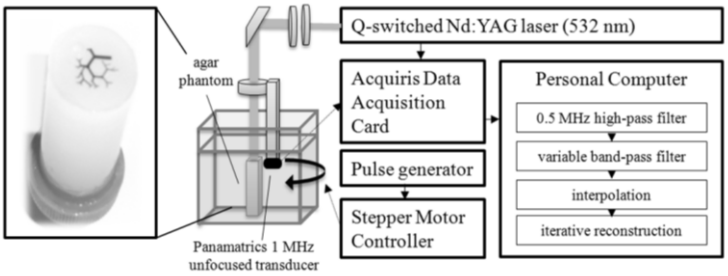

| **Figure 2** – Schematic representation of the photoacoustic tomographic setup and the signal processing (including an image of the agar phantom).

MATERIALS AND METHODS

Simulations

To simulate PA experiments done using the imaging set-up, a HPI algorithm was designed using Matlab (Mathworks Inc., 2011b, Natick, MA) and the k-Wave toolbox [8]. The forward simulated pressure signals for an ideal (broadband, infinite small aperture) detector were convolved with the frequency response of the detector (see next section) to mimic real-world signals. These time traces were used for time reversal reconstruction [3].

Detector characterization

The detector was characterized to assess its frequency response. A commercially available, 1 MHz piezoelectric unfocused transducer (Panametrics–NDT, V303, .5", 521400) was used. A hydrophone setup was built, in which a broadband needle hydrophone (Precision Acoustics, Ltd.) and the detector were placed 10 cm apart in a water tank. The detector was driven by a negative square, broadband pulse (–100 V, 0.5 μs), using a pulse/receiver (Panametrics, 5077PR) and the acoustic signal was detected by the hydrophone that was considered equally sensitive to a broad range of frequencies. The signal (f_s = 500 MHz, averaged over 1000 signals) was recorded using a data acquisition card (Acqiris 8-bit 500 ms/s) after amplification (DC Coupler, Precision Acoustics, DCPS186). Using fast Fourier transform the frequency response was obtained.

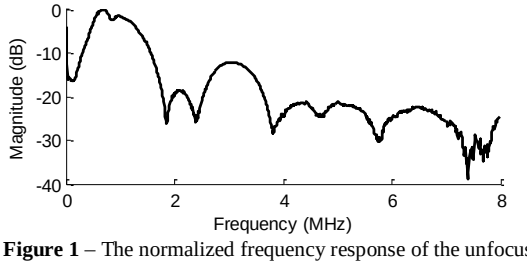

| **Figure 1** – The normalized frequency response of the unfocused 1 MHz transducer (Panametrics).

Phantoms

A two-dimensional phantom was produced, by laserprinting a vasculature-like phantom design on a < 150 μm thick transparent polyester sheet (Xerox, 003R98220). The black toner (Xerox, 006R01449) has a high light absorbance, while the foil has a low light absorbance for the visible wavelength range. Printing was done with a resolution of 1200 dpi (dots per inch, corresponding to 0.021 mm/pixel). After printing, the sheet was incorporated on top of a cylindrical shaped 2 w/v-% agar phantom.

Photoacoustic tomography imager

The experiments were performed in a top illumination PA tomography setup that consisted of an imaging tank with water in which the agar phantom was placed, with the printed structure facing upward (**Figure 2**) [9]. The 1 MHz transducer was attached to a mechanical arm that was rotated around the sample with a radius of approximately 32 mm, using a stepper motor. The phantom was illuminated from the top with a laser beam aligned with mirrors and expanded using two lens systems to a diameter of circa 12 mm. To homogeneously distribute the light, the water basin was filled with a diffusing 0.1 % Intralipid solution. The laser beam was produced by a Q-switched Nd:YAG laser (Quantel, Brilliant B, France) with a wavelength of 532 nm by second harmonic generation (10 Hz pulse frequency, 5 ns, energy 130 mJ per pulse).

The measurement protocol discussed in [9] and [10], requires a calibration measurement on an object which carries two or more landmark absorbers. We used a cylindrical agar phantom, with the same dimensions as the phantom under investigation, in which three horsetail hairs were embedded. This calibration phantom was imaged with 180 projections, each 2° apart. Then the vasculature phantom was scanned with 240 projections of 1.5°.

Image reconstruction

All datasets were first high-pass filtered with a cut-off frequency of 0.5 MHz using a second order Butterworth filter to remove the off-set and reduce low-frequency artifacts. Then we used a second order Butterworth variable band-pass filter to isolate only the fundamental FBW (0–2 MHz) or the harmonic frequencies (2–7 MHz). The signals from these frequency bands were model-based iteratively

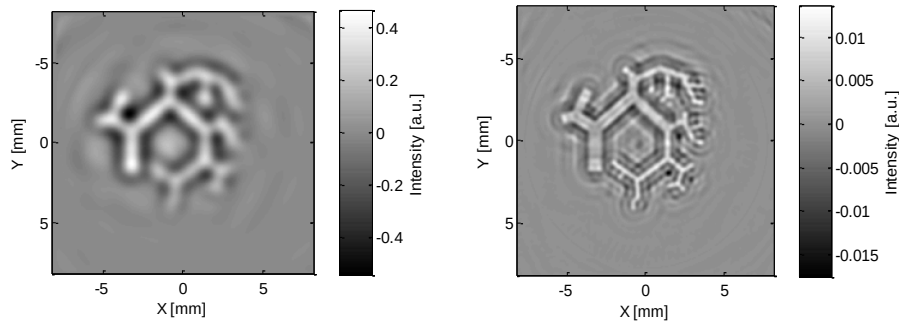

| **Figure 3** –Digitally, characterized transducer k-Wave simulations were performed after filtering with **(left)** bandwidth 0–2 MHz (fundamental FBW image) and **(right)** bandwidth 2–7 MHz (harmonic FBW image).

reconstructed using a PA imaging program in Matlab [11], to yield two images: the conventional fundamental frequency image and the 'harmonic' image. After reconstruction, the adjustable parameters giving the best image result were chosen to optimize image quality; L1 norm total variation regularization, using a smoothness constant λ of 2, the number of iterations was set to 25 and there was no preconditioning applied [11].

The HPI approach

In HPI, information from both images needs to be combined. Due to a difference in intensities between them – the 'harmonic' image possesses lower values – we normalized the reconstruction data by dividing the image values by the maximum intensity, as a first simple method to bring both images in the same intensity range. Subsequently, the sum of both normalized images was taken. This approach of combining the normalized images will be called the HPI approach.

Spatial resolution of the images was defined by the zero-crossing widths of the positive main lobes in the image profile [6,12]. As the convolution between the point spread function (PSF) of the experimental system and the dimensions of the imaged object itself determine the size of the image, a comparison between the original size and the zero-crossing widths of the image determine spatial resolution [6].

RESULTS AND DISCUSSIONS

In **Figure 1** the detector's frequency response is displayed. It is seen that band-pass filters of 0–2 MHz and 2–7 MHz would only include the contributions of the fundamental FBW and the harmonics, respectively. Higher frequencies will not contribute to the signal, since their contributions are below -20 dB, making them too sensitive to noise. High-pass filtering from 0.5 MHz is justified, as this is the -6 dB border of the fundamental FBW.

The simulations on a 700x700 (22 μm pixels) grid are presented in **Figure 3**. In the fundamental FBW (left) the phantom structure is well reconstructed while the thinner branchers appear blurred as expected. These thinner 'vessels' are faithfully reconstructed in the 'harmonic' image (right), while the edges of larger 'vessels' are delineated.

In **Figure 4a–b** two iterative reconstructions of the experimental data for the same FBWs, performed on a grid of 1600x1600 pixels with width 8.3 μm, are shown. The same effects as in the numerical simulations are observed. Because the absorption of the phantom was not known, the absolute values of the pressure distribution cannot be compared. As for the pressure distribution, intensity values seem to correspond.

Some general but important remarks regarding the images can be made. First, it should be noted that the image intensities in the harmonic images are considerably smaller than the fundamental images. This is because the detector is more sensitive to its fundamental frequency than its higher harmonics (**Figure 1**). Second, further from the center of rotation, the images have worse resolutions. This is considered the effect of the finite-sized illumination beam, which is weaker in

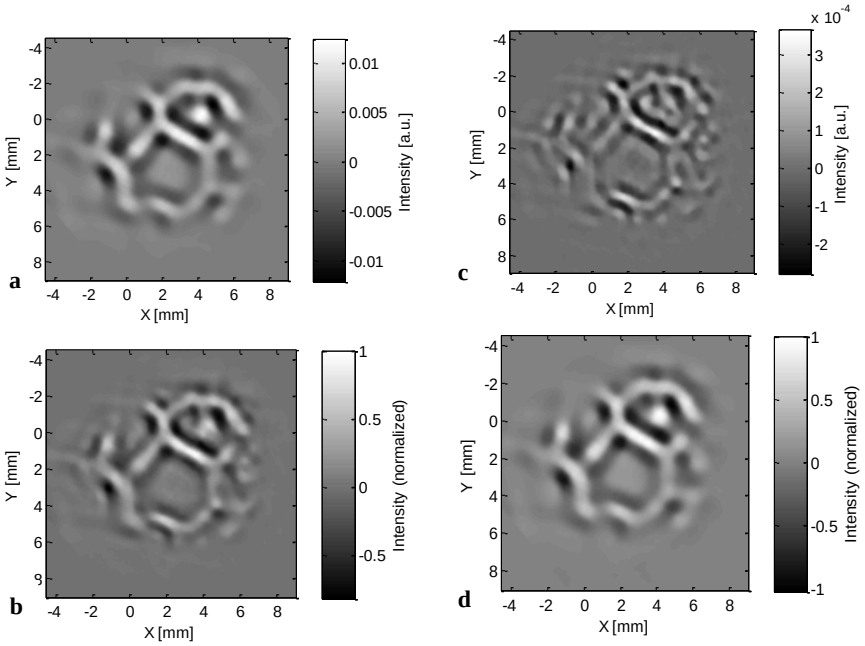

| **Figure 4**–Experimental iterative reconstructions of the vasculature phantom, filtered with **(a)** bandwidth 0–2 MHz (fundamental FBW image) and **(b)** bandwidth 2–7 MHz (harmonic FBW image). In **(c)** these reconstructions were normalized and added together. Also, **(d)** an experimental reconstruction after filtering with bandwidth 0–7 MHz is included.

| **Table 1** – Image zero-crossing widths in the reconstruction image, measured in the cross section shown in the right-hand image.

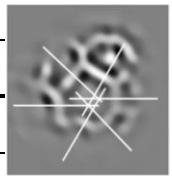

reconstruction	zero-crossing width (mm)					
	1 mm vessel	0.75 mm vessel	0.56 mm vessel	0.42 mm vessel	0.31 mm vessel	0.24 mm vessel
conventional	0.92	0.94	0.76	0.78	0.78	0.81
HPI	0.91	0.76	0.63	0.50	0.63	0.62

those regions. Moreover, the large area detector has narrow acceptance angle, which reduces the lateral resolution of the PA tomography system [13].

The HPI image was compared to the normalized reconstruction of the signal filtered with bandwidth 0–7 MHz, but without enhancement of the harmonic signal (**Figure 4c and d**). In **Table 1** the zero-crossings of the imaged vessels (see inset figure) are displayed. Almost all vessels in the HPI image possess zero-crossing widths that are closer to the real size compared to the fundamental FBW image, especially the smaller vessels. This demonstrates that a higher resolution is achieved as a result of the HPI approach. To enhance this effect, it is recommended, as harmonic resonances are more sensitive to noise due to their low intensities, to physically enhance these harmonics in the US detectors. Also, it is preferable to look at the deconvolution method for each harmonic specifically. This procedure may improve image quality.

CONCLUSIONS

In this research, the concept of harmonic PA imaging was presented and demonstrated using both simulation and experiments. A two-dimensional phantom was designed and implemented, and was imaged in a PA tomography setup with an unfocused 1 MHz detector. The PA signals were filtered with a band-pass of 0–2 MHz and 2–7 MHz, therefore including only the contributions of the detector's fundamental frequency and its harmonics, respectively. The harmonic images clearly showed enhanced edges for bigger structures, and lines as a whole for the smaller ones. Appropriately combining the fundamental image and the harmonic image, an HPI image was produced. In this image, line widths were reconstructed closer to the real sizes than in the corresponding 0–7 MHz band-pass filtered image reconstruction.

Hence, enhancing the contribution of the detector's harmonics can be used to improve image quality (i.e. spatial resolution). The method permits achieving higher resolutions than conventionally thought of, without requiring challenging engineering modifications otherwise necessary. Further, with the use of specialized compounding schemes to combine HPI data while penalizing noise, we believe that the method can be made applicable to various implementations of photoacoustics from microscopy to breast imaging. Future work will focus on developing more sophisticated methods for data combining, and the approach will be applied to more challenging phantoms and biological samples.

REFERENCES

1. Wang, L.V. Multiscale photoacoustic microscopy and computed tomography. *Nature Photon. 3*, 9 (2009), 503-509.
2. Wang, L.V. and Hu, S. Photoacoustic Tomography: In Vivo Imaging from Organelles to Organs. *Science 335*, (2012), 1458-1462.
3. Treeby, B.E., Zhang, E.Z. and Cox, B.T. Photoacoustic tomography in absorbing acoustic media using time reversal. *Inverse Problems 26*, 11 (2010).
4. Manohar, S. *et al.*, The Twente Photoacoustic Mammoscope: System overview and performance. *Phys. Med. Biol. 50*, 11 (2005), 2543-2557.
5. Xu, M. and Wang, L.V. Analytic explanation of spatial resolution related to bandwidth and detector aperture size in thermoacoustic or photoacoustic reconstruction. *Phys. Rev. E 67*, 52 (2003), 1-15.
6. Ku, G. *et al.*, Multiple-bandwidth photoacoustic tomography. *Phys. Med. Biol. 49*, 7 (2004), 1329-1338.
7. Wang, X. *et al.*, Photoacoustic tomography of biological tissues with high cross-section resolution: Reconstruction and experiment. *Med. Phys. 29*, 12 (2002), 2799-2805.
8. Treeby, B.E. and Cox, B.T. k-Wave: MATLAB toolbox for the simulation and reconstruction of photoacoustic wave fields. *Journal of Biomedical Optics 15*, 2 (2010).
9. Jose, J. *et al.*, Passive element enriched photoacoustic computed tomography (PER PACT) for simultaneous imaging of acoustic propagation properties and light absorption. *Opt. Expr.19*, 3 (2011), 2093-2104.
10. Willemink, R.G.H. et al., A Fast Iterative Reconstruction Method using Preconditioning for Photoacoustic Computed Tomography, 2012, *under review*.
11. Willemink, R.G.H. Image reconstruction in a photoacoustic element enriched photoacoustic setup. PhD Thesis, BMPI, Twente University, Enschede, 2010.
12. Ku, G. and Wang, L.V. Deeply penetrating photoacoustic tomography in biological tissues enhanced with an optical contrast agent. *Opt. Lett. 30*, 5 (2005), 507-509.
13. Li, C., Ku, G., and Wang, L.V. Negative lens concept for photoacoustic tomography. *Phys. Rev. E 78*, 2 (2008), 021901.